Food Chemistry 351 (2021) 129340

Contents lists available at ScienceDirect

Food Chemistry

journal homepage: www.elsevier.com/locate/foodchem

Preparation, structure characterization, and specific gut microbiota properties related to anti-hyperlipidemic action of type 3 resistant starch from *Canna edulis*

Chi Zhang [a,b,c], Minyi Qiu [a,d], Ting Wang [b], Linglong Luo [a], Wenjuan Xu [a], Jiahui Wu [a], Fangyuan Zhao [a], Kaiyang Liu [a], Yuan Zhang [c,*], Xueyong Wang [a,b,*]

[a] School of Chinese Materia Medica, Beijing University of Chinese Medicine, No.11 North 3rd Ring East Road, Chao-Yang District, Beijing 100029, China
[b] Beijing Research Institute of Chinese Medicine, Beijing University of Chinese Medicine, Chao-Yang District, Beijing 100029, China
[c] College of Biochemical Engineering, Beijing Union University, No. 18, Fatou Xili District, Chaoyang District, Beijing 100023, China
[d] Pharmacy Department, Peking University People's Hospital, No. 11, Xizhimen Street, Xicheng District, Beijing 100044, China

ARTICLE INFO

Keywords:
Type 3 resistant starch
Canna edulis
Structural properties
Anti-hyperglycemia
Gut microbiota
Prebiotic

ABSTRACT

Type 3 resistant starch (RS3) was developed from *Canna edulis* (Ce) native starch (NS) through dual enzymatic hydrolysis and recrystallization. Thereafter, the processed Ce-RS3 was subjected to systematic characterizations for its structural properties, anti-hyperlipidemic effect, and *in vivo* gut microbiota modulatory function.

The Ce-RS3 content was increased to 49.11% after processing under optimal conditions. Compared with NS, Ce-RS3 maintained its B-type crystallization without introducing new chemical groups. Meanwhile, it displayed coarse surfaces, higher crystallinity, more ordered structures, and a higher proportion of chains with degree of polymerization (DP) 37-100. Ce-RS3 intervention significantly alleviated dyslipidemia in hyperlipidemic mice, which was associated with increased gut microbial diversity and unique microbial enrichment, potentially mediated by its fine structure. These observations are valuable for developing RS3 from *C. edulis* for prebiotics applications and support the potential strategy that utilizes well-designed RS to modulate specific bacterial populations to improve health.

1. Introduction

Resistant starch (RS) is a special type of processed starch from starches and its degradation products that possess enzymatic resistance after processing (Bindels, Walter, & Ramer-Tait, 2015). Based on its processing methods and physical inaccessibility, RS can be generally classified into four types, namely RS1-4 as physically-embedded, raw-granular, retrograded, and chemically-modified starches, respectively. Unfortunately, RS1 and RS2 can lose their anti-digestion properties during grinding, cooking, and puffing; meanwhile, RS4 is usually processed by chemical reagents that are potential safety hazards for humans (Bindels, Walter, & Ramer-Tait, 2015). In contrast, RS3 is formed during food processing without using toxic reagents, which has advantages of thermal stability, controllable production, and stable anti-enzymatic hydrolysis properties (Jiang, Du, Jiang, Wang, & Du, 2019). Therefore, RS3 has the most potential widespread application in the food industry.

In addition to common potato, corn, and cassava starch materials, other sources of raw starch such as brown lentil and buckwheat have recently been developed for the production of RS (Jiang, Du, Jiang, Wang, & Du, 2019); however, there is limited information about RS deriving from *Canna edulis*. Zhang and Wang (2009) prepared RS from *C. edulis* by phosphorylation, and found that the phosphorylation destroyed the original starch structure with a transformation of the crystallization from type B to type A. This group also prepared *C. edulis*-derived RS by heat-moisture treatment, and measured changes in starch structure during digestion *in vitro* (Zhang, Chen, Liu, & Wang, 2009). However, these studies have suffered from cumbersome processes, complex instrument requirements and potential safety hazards, limiting the development and industrial production of *C. edulis*. *C.edulis* was

* Corresponding authors at: College of Biochemical Engineering, Beijing Union University, No. 18, Fatou Xili District, Chaoyang District, Beijing 100023, China (Y. Zhang). School of Chinese Materia Medica, Beijing University of Chinese Medicine, No.11 North 3rd Ring East Road, Chao-Yang District, Beijing 100029, China (X. Wang).
E-mail addresses: zhangyuan333@buu.edu.cn (Y. Zhang), xueyongwang@bucm.edu.cn (X. Wang).

https://doi.org/10.1016/j.foodchem.2021.129340
Received 26 May 2020; Received in revised form 27 January 2021; Accepted 8 February 2021
Available online 20 February 2021

originated in South America and now widely distributed in China, Thailand, Vietnam, and other countries (Hung & Morita, 2005). Dry rhizomes of *C. edulis* contain 70–80% starch, with higher amylose content and proportion of long branch chains than commercial cassava and potato starches (Hung & Morita, 2005). Given these structural features, *C. edulis* may be a promising source of RS for industrial production and commercial development. Therefore, it is important to develop a simple, green approach for industrial production of RS, especially RS3, from *C. edulis*.

One of the attractive options for preparing RS3 is through enzymatic degradation, which can safely and simplicity release linear starch fragments with greater fluidity, thereby achieving recrystallization. For example, pullulanase can hydrolyze the α-1,6 glycosidic bonds in starch and release a large proportion of linear glucan chain, which improves RS3 production (Shi, Chen, Yu, & Gao, 2013). Amylase can hydrolyze the α-1,4 linkages of starch chains, thereby generating a larger proportion of linear chains with suitable chain length, enhancing the retrogradation of starch to increase the RS3 content (Villas-Boas & Franco, 2016; Zhang & Jin, 2011). Thus, the use of a combination of amylase and pullulanase may be a safe, efficient and simple method to enrich more linear chains in starch granules to obtain RS3. However, starches from various plant sources undergo different hydrolysis reactions (Villas-Boas & Franco, 2016), while no study has reported the enzymatic modification of *C. edulis*-derived RS3 or characterized its physicochemical properties.

There is a growing awareness of the prebiotic properties of RS (Zaman & Sarbini, 2015). However, most of the studies were focused on *in vitro* prebiotic effects of RS on gut microbiota, while little evidence has been found *in vivo* (Gu, Li, Hamaker, Gilbert, & Zhang, 2020; Zeng et al., 2018; Zhang, Zeng, Wang, Zeng, & Zheng, 2014). In addition, previous studies have shown that different types of RS, derived from various sources and with distinct chemical structures, can promote the growth of different types of gut microorganisms, which further affected its biological activity (Bindels, Walter, & Ramer-Tait, 2015; Gu, Li, Hamaker, Gilbert, & Zhang, 2020; Xu, Ma, Li, Liu, & Hu, 2020). Our previous study found ameliorative effects of RS from *C. edulis* on metabolic diseases (Zhang et al., 2020). However, the *in vivo* gut microbiota-modulatory, anti-hyperlipidemic effect, and its potential relationship with structure of Ce-RS3 have not been characterized.

In this study, RS3 from *C. edulis* was prepared by dual enzymatic (i.e. amylase and pullulanase) modification and recrystallization. Response surface methodology (RSM) was applied to optimize the reaction parameters for improving RS content. The structures, structural properties, *in vivo* anti-hyperlipidemic effect and microbiota-regulatory effect of Ce-RS3 were characterized.

2. Materials and methods

2.1. 2.1Materials

Canna edulis native starch was obtained from Yilitai Biotechnology Co., Ltd. (Guizhou, China). Pullulanase (1,000 ASPU/ml) was purchased from Novozymes Investment Co. Ltd. (Beijing, China). High-temperature α-amylase (1,0000 U/g) was acquired from Solarbio Co. Ltd. (Beijing, China). Potato amylose standards, amyl glucosidase, porcine pancreatic alpha-amylase were provided by Sigma Co., Ltd (St. Louis, MO, USA). D-Glucose assay kit was obtained from Megazyme International Ltd. (Co. Wicklow, Ireland). The Milli-Q system (Millipore Corporation, MA, USA) was used to purify deionized water. Simvastatin hydrochloride was provided by Sino-US Shanghai Squibb Pharmaceutical Co., Ltd. The other reagents and chemicals were all analytical grade.

2.2. Structural properties

2.2.1. Response surface methodology (RSM)

RSM was carried out with the Design Expert (v8.06) software. A four-factor, three-level Box Behnken design (Table 1) was performed to investigate the influencing factors of Ce-RS3. Four independent factors, including α-amylase dosage (X1), α-amylase hydrolysis time (X2), pullulanase dosage (X3), and pullulanase hydrolysis time (X4), were used as variables and studied at low (-1), middle (0), and high (1) levels, respectively. These variables and their respective levels were as follows: 0, 2, and 4 U/g for X1; 10, 15, and 20 min for X2; 2, 4, and 6 U/g for X3; 6, 8, and 10 h for X4. The Box Behnken design generated a total of 29 experiments. The horizontal coding ranges of the respective variables are shown in Table S1. The design matrix for model coding and prediction is shown in Table S2. The significance of correlations among factors in the model was determined based on analysis of variance (ANOVA) (Table 1), and the appropriate model was finally selected for optimization.

2.2.2. Preparation of the retrograded starch

An aliquot of 15 g *C. edulis* native starch was dispersed into 100 mL phosphate buffer solution (pH 5.5) and fully gelatinized in boiling water for 20 min. Thereafter, high-temperature α-amylase was added and stirred at 200 rpm. The temperature of the boiled starch was adjusted to 58 °C, and the pH was adjusted to 4.8, followed by adding pullulanase immediately for incubation. Subsequently, the starch paste was cooled down to room temperature and preserved at 4 °C for 12 h to retrograde. Finally, the recrystallized starch was collected by centrifugation at 3,000 rpm, dried at 50 °C, ground, and filtered with a 200-mesh sieve for further analyses.

2.2.3. RS and amylose content of NS and Ce-RS3

The contents of amylose in the native starch and Ce-RS3 were determined by an iodine colorimetric method (AOAC International, 2007). RS concentration was determined following the AOAC approach

Table 1
ANOVA results for the response surface quadratic model for Ce-RS3.

Source	Sum of squares	df	Mean Square	F-Value	p-value	Remarks
Model	610.39	14	43.6	45.2	< 0.0001	significant
X_1	8.31	1	8.31	8.61	0.0109	significant
X_2	2.31	1	2.31	2.39	0.144	
X_3	109.43	1	109.43	113.44	< 0.0001	significant
X_4	52.9	1	52.9	54.84	< 0.0001	significant
X_1X_2	1.21	1	1.21	1.25	0.2818	
X_1X_3	7.92	1	7.92	8.21	0.0125	significant
X_1X_4	0.039	1	0.039	0.041	0.8433	
X_2X_3	4.51	1	4.51	4.67	0.0485	significant
X_2X_4	1.3	1	1.3	1.35	0.2648	
X_3X_4	4.28	1	4.28	4.44	0.0536	
X_1^2	195.21	1	195.21	202.38	< 0.0001	significant
X_2^2	63.25	1	63.25	65.57	< 0.0001	significant
X_3^2	252.26	1	252.26	261.52	< 0.0001	significant
X_4^2	109.68	1	109.68	113.71	< 0.0001	significant
Residual	13.5	14	0.96			
Lack of Fit	10.2	10	1.02	1.23	0.4542	not significant
Pure Error	3.31	4	0.83			
Cor Total	623.89	28				

$R^2 = 0.9784$ R^2-Adj $= 0.9567$.
Experimental values corresponding to optimization results = 49.11(±0.42)%.

(AOAC International, 2007). More details are given in Supplementary Method.

2.2.4. Characterization of NS and Ce-RS3

The composition, water binding capacity (WBC), paste transparency, swelling power, and solubility of NS and Ce-RS3 were determined according to published strategies. Detailed methodology is provided in the Supplementary Method. The morphology of NS and Ce-RS3 was visualized by the field emission scanning electron microscope (SEM) (FE-TEM, JEM-2100, Japan). The X-ray diffraction (XRD) patterns of starch samples were recorded by the XRD image processor (Bruker, D8 advance, Germany) with current and voltage at 40 mA and 40 kV, respectively. Sample pieces were scanned by the IR spectrophotometer (PerkinElmer, Waltham, USA), using the purified potassium bromide piece as the background. The Chain-length distributions of NS and Ce-RS3 were analyzed by a high-performance size-exclusion chromatography (HPSEC) system (AcQuity UPLC, Waters, USA) coupled with a Optilab *T*-rEX refractive index detector (RID, Wyatt Technology, CA, USA). The Supplementary Methods give the details of all the procedures.

2.3. Animals experiments

Six-week-old male ICR mice (n = 30, 28 ± 2 g) were provided by Beijing Weitong Lihua Experimental Animal Technology Co., Ltd. (certificate number SCXK (Beijing) 2016–0006), and raised in an animal room with barrier facility in Beijing University of Chinese Medicine (animal license number: SYXK (Beijing) 2016–0038). All the mice had free access to water and feed. The feeding conditions were: Room temperature at 23 ± 2 °C, relative humidity at 40%-70%, and daylight for 12 h. All the animal procedures were complied with the regulations of the National Institutes of Health (NIH), and conducted under the guidance of the Animal Ethics Committee of Beijing University of Chinese Medicine (No. BUCM-4–2018060421-2025). After 7 days of acclimatization, the mice were randomly divided into normal control group (Control, n = 6) and hyperlipidemic diet group (n = 24). The mice in the control group were fed with standard diet, while the other mice were fed with high-fat diet (HFD; 20% protein, 35% carbohydrate, and 45% fat) for 8 weeks. The HFD-fed mice were considered hyperlipidemic when their total triglyceride (TG) and total cholesterol (TC) levels in serum were significantly higher from those of the control group. Then, the hyperlipidemic mice were further randomly divided into four subgroups (n = 6 per group) with the following treatments for 12 weeks: Model group (Model), simvastatin group (simvastatin, 0.004 g/kg), high-dose RS group (L_Ce-RS3, 3 g/kg), and low-dose RS group (L_Ce-RS3, 1.5 g/kg). Ce-RS3 was prepared under the closest optimal conditions designed by RSM, using the following parameters: α-amylase dosage (2 U/g), α-amylase hydrolysis time (15 min), pullulanase dosage (4 ASPU/g), and pullulanase hydrolysis time (8 h). The prepared Ce-RS3 was suspended in water and administered to the interventional group by oral gavage. The mice in the control and model groups were given an equal volume of distilled water.

2.4. Serum biochemical indicators and Histopathological(H&E) analysis

The serum levels of TG, TC, total high-density lipoprotein cholesterol (HDL-C), and total low-density lipoprotein cholesterol (LDL-C) were measured by an automatic biochemical analyzer (AU480, Beckman Coulter, USA). Fat and liver tissues sections were subjected to hematoxylin and eosin (H&E) staining. An optical microscope (Olympus, Tokyo, Japan) was used for histological analysis. The sizes of adipocytes were estimated using the Image-Pro Plus software (IPP, version 6.0, Media Cybernetics, USA).

2.5. DNA extraction and 16S rRNA sequencing

Total DNA was extracted using the QIAamp Fast DNA Stool Mini Kit, and the DNA concentration was measured by the Nanodrop 2000 spectrophotometer (Thermo Scientific, USA). PCR was conducted to amplify the V3-V4 regions of bacterial 16S rDNA, using the following primers: 338F (5′-ACTCCTACGGGAGGCAGCAG-3′, forward) and 806R (5′-GGACTACHVGGGTWTCTAAT-3′, reverse). Alpha-diversity indicators, including Chao1 and Shannon indices, were determined for species richness based on the OTUs table. Additionally, beta-diversity indices among samples were visually measured by principal coordinate analysis (PCoA) based on the UniFrac distance, according to the OTUs degree. Furthermore, the taxa of intestinal biomarkers were identified by linear discriminant analysis (LDA) effect size (LEfSe).

2.6. Statistical analysis

The values were presented as mean ± standard deviation (SD). Statistical analyses were conducted using the GraphPad Prism 8.0 (GraphPad Software, San Diego, USA). Differences among groups were analyzed by Students'*t*-test or one-way ANOVA followed by Tukey's test, and statistical significance was determined based on $p < 0.05$. Intestinal microflora characteristics were identified by Kruskal-Wallis (KW) rank sum test and LEfSe analysis, and statistical significance was determined based on $p < 0.05$ and LDA > 2.5.

3. Results and discussion

3.1. Structure characterization

3.1.1. RSM for Ce-RS3 productivity.

To maximize productivity, the four variables (X1-4) were transformed to coded values, with Ce-RS3 content considered as the dependent variable to predict responses (Table S1). Twenty-nine different experiments were performed based on a four-factor Boxe-Behnken design. The detailed experimental plan is shown in Table S2. Table 1 shows the effects of these variables and their potential interactions based on ANOVA. The second-order polynomial equation describing the relationship between the significant variables and Ce-RS3 content (Y) is as follows:

$$Y = 48.29 + 0.83X_1 - 0.44X_2 - 3.02X_3 - 2.1X_4 - 0.55X_1X_2 - 1.41X_1X_3 - 0.099X_1X_4 - 1.06X_2X_3 - 0.57X_2X_4 - 1.03X_3X_4 - 5.49X_1^2 - 3.12X_2^2 - 6.24X_3^2 - 4.11X_4^2$$

where Y is the experimental response and Xi is the significant independent variables.

The *p*-value of the adjusted model indicated a significant statistical difference ($p < 0.0001$), and the adjusted model exhibited a good fit with statistical significance ($p = 0.4542$), indicating that the obtained model was well adapted to the response. Moreover, the fairly high R^2 value (0.9784) and adjusted correlation coefficient (Adj-R^2, 0.9567) demonstrated that the model possessed good adaptability to the capture efficiency. The *p*-values of X1, X3, X4, X_1^2, X_2^2, X_3^2, and X_4^2 were all<0.05, indicating that they were the significant influencing factors for the response. Meanwhile, X_1X_3 was also a significant factor ($p = 0.0125$), suggesting a significant interaction between α-amylase and pullulanase

dosages. Pullulanase is a debranching enzyme that specifically hydrolyzes α-1,6 glycosidic bonds, while α-amylase shortens the chain length of starch molecules. These results supported the conclusion that double enzymatic hydrolysis by amylase and pullulanase can form a larger proportion of linear starch molecules with a suitable chain length, which facilitates their recrystallization (Villas-Boas & Franco, 2016).

Based on the Box-Behnken design, the optimal processing conditions were 2.22 U/g α-amylase hydrolysis for 14.9 min and 3.53 ASPU/g pullulanase hydrolysis for 7.55 h, which would achieve a predicted RS3 content of 48.92%. Under these conditions, the corresponding experimental Ce-RS3 was 49.11%, which was in line with the predicted value (Table 1).

3.1.2. Physicochemical properties of Ce-RS3

The content of RS3 prepared under the optimal conditions was not significantly different from that under the closest conditions. To facilitate actual production, subsequent experiments were carried out using the closest optimal processing conditions of : 2 U/g α-amylase hydrolysis for 15 min and 4 ASPU/g pullulanase hydrolysis for 8 h. The RS content greatly increased from 5.87% (native starch) to 48.23% (Ce-RS3), which was in accordance with the predicted value (Tables 2 and S2). After modification, the physicochemical properties of Ce-RS3 were changed (Table 2). The amylose content of *C. edulis* native starch was 26.98%, which was higher than commercial cassava starches reported in previous literature (Hung & Morita, 2005). Compared to NS, the amylose content of Ce-RS3 increased significantly, to 31.03%. This may be caused by the hydrolysis of amylose and long amylopectin of NS by α-amylase and pullulanase under appropriate conditions. Amylose has a strong tendency to recombine and reverse transcripts more easily, resulting in more RS3 (Gidley & Bulpin, 1989; Shi, Chen, Yu, & Gao, 2013). These results indicated that *C. edulis* is a promising source for preparing RS3. The protein, fat and ash contents of Ce-RS3 were significantly lower than those of native starch, indicating the destruction of structure during processing. The WBC of RS is mainly related to the hydrogen bonding between starch chains. More hydrogen bonds and covalent bonds inside the molecule are associated with less water binding sites, resulting in a lower WBC. After processing, the WBC of Ce-RS3 was significantly enhanced from 66.7% to 186.78%, and the paste clarity was also increased from 1.26 to 1.45%. These might be related to the increased hydrophilic groups and decreased hydrophobic groups during processing. Similar results were observed by Mao et al. (2018).

The swelling power and solubility of native starch and Ce-RS3 at five different temperatures (55, 65, 75, 85, and 95 °C) are shown in Fig. S1A and B, respectively. Swelling power and solubility can be assessed to evaluate the degree of interaction between starch chains, specifically within the amorphous and crystalline domains (Singh, Inouchi, & Nishinari, 2006). With an increased temperature, the swelling power and solubility of Ce-RS3 and native starch were increased, indicating that the starch molecules combined with water molecules were heat-activated for gelatinization. Interestingly, Ce-RS3 exhibited greater swelling power and solubility at lower temperatures (55 and 65 °C), but more stable properties at higher temperatures (85 and 95 °C). These might be attributed to the release of a large number of linear glucan chains under dual enzymatic conditions, forming stable crystals through hydrogen bonding (Villas-Boas & Franco, 2016). The ordered double-helical structure of Ce-RS3 enhanced the interactions between starch chains at amorphous and crystalline regions, prevented the release of more starch chains at high temperature, which ensured Ce-RS3 with a better thermal stability (Genkina, Wikman, Bertoft, & Yuryev, 2007). However, enzymatic hydrolysis was also accompanied by the release of a number of short linear glucan chains that failed to form crystals, which increased the swelling power and solubility at lower temperatures (Gidley & Bulpin, 1989; Li, Yuan, & Ai, 2020).

3.1.3. Scanning electron micrographs

We observed that the granules of native starch were round or oval in shape with an average diameter of ~ 30 μm, and they were smooth surfaced without striation cracks (Fig. 1A, B, and C). Although Ce-RS3 granules maintained their complete particle structures, the smooth surface was compromised during processing, exhibiting irregular, compact, flaky structures (Fig. 1D, E, and F). The structural changes might be attributed to the effects of amylose and amylopectin recrystallization, by which the starch molecules were rearranged close to each other through hydrogen bonding, resulting in a recombination of mixed dimensional crystal bundles, thus preventing the formation of spherulites (Cai & Shi, 2013). During this process, Ce-RS3 formed a compact block structure, and with the leaching of amylose, an irregular sheet structure was formed on the surface. Tight microstructure morphology has been reported to increase the resistance to enzyme attack and alter the microbiota response to resistant starches (Gu, Li, Hamaker, Gilbert, & Zhang, 2020; Ma & Boye, 2018; Zeng et al., 2018). These changes suggested that Ce-RS3 might exhibit improved gut microbiota fermentation properties.

3.1.4. FT-IR analysis

FT-IR is an effective method to monitor starch structural changes during processing. Fig. 2A shows the FT-IR spectrum of native starch and Ce-RS3. The absorption bands at 995 and 1047 cm^{-1} related to the ordered structure of starch and sensitivity to crystallinity, while the absorption band at 1022 cm^{-1} represented the amorphous regions (Ma & Boye, 2018). The 995/1022 cm^{-1} and 1047/1022 cm^{-1} band ratios were representative and sensitive indices for quantifying the order degree of starch samples, with a higher ratio representing a higher proportion of crystalline regions (Ma & Boye, 2018). IR spectral analysis showed that the ratios of 995/1022 cm^{-1} and 1047/1022 cm^{-1} bands of native starch were 0.946 and 0.982, while those of Ce-RS3 were 1.04 and 1.21, respectively. These results indicated that the degree of crystallinity of Ce-RS3 was higher than that of native starch, which was further confirmed by XRD analyses. The absorption bands in the region of 3100–3700 cm^{-1} are quite sensitive to the structural changes of hydrogen bonds (Ma & Boye, 2018), and Zhang, Zeng, Wang, Zeng, and Zheng (2014) observed more precise inter-and intra-molecular hydrogen bonds during gelatinization and retrogradation, resulting in narrowing amplitude. Consistent with this finding, the amplitude of Ce-RS3 was significantly narrowed in the absorption region of 3100–3700 cm^{-1}, which was significantly different from the pattern observed for NS. These results illustrated that Ce-RS3 subjected to dual enzyme treatment had more precise hydrogen bonding changes during gelatinization and retrogradation.

3.1.5. Crystallinity patterns

The XRD patterns revealed that native starch generated strong

Table 2
Protein, Lipid, Ash, moisture, resistant starch (RS), water-binding capacity (WBC), paste clarity, relative crystallinity and amylose content of NS and Ce-RS3. $^{*}p < 0.05$, $^{**}p < 0.01$ Ce-RS3 versus the NS. Except for moisture content, other traits were expressed in dry wt basis.

Samples	Protein (%)	Lipid (%)	Ash (%)	Amylose content (%)	Moisture (%)	RS (%)	WBC (%)	Paste clarity (%)	Relative crystallinity (%)
NS	0.18 ± 0.02	0.52 ± 0.02	0.36 ± 0.02	26.98 ± 0.36	13.07 ± 0.68	5.8%±0.50	66.70 ± 2.67	1.26 ± 0.02	34.71
Ce-RS3	0.04 ± 0.00**	0.37 ± 0.02**	0.20 ± 0.01**	31.03 ± 0.24*	2.75 ± 0.29**	48.23%± 1.20**	186.78 ± 0.80**	1.73 ± 0.05*	39.40

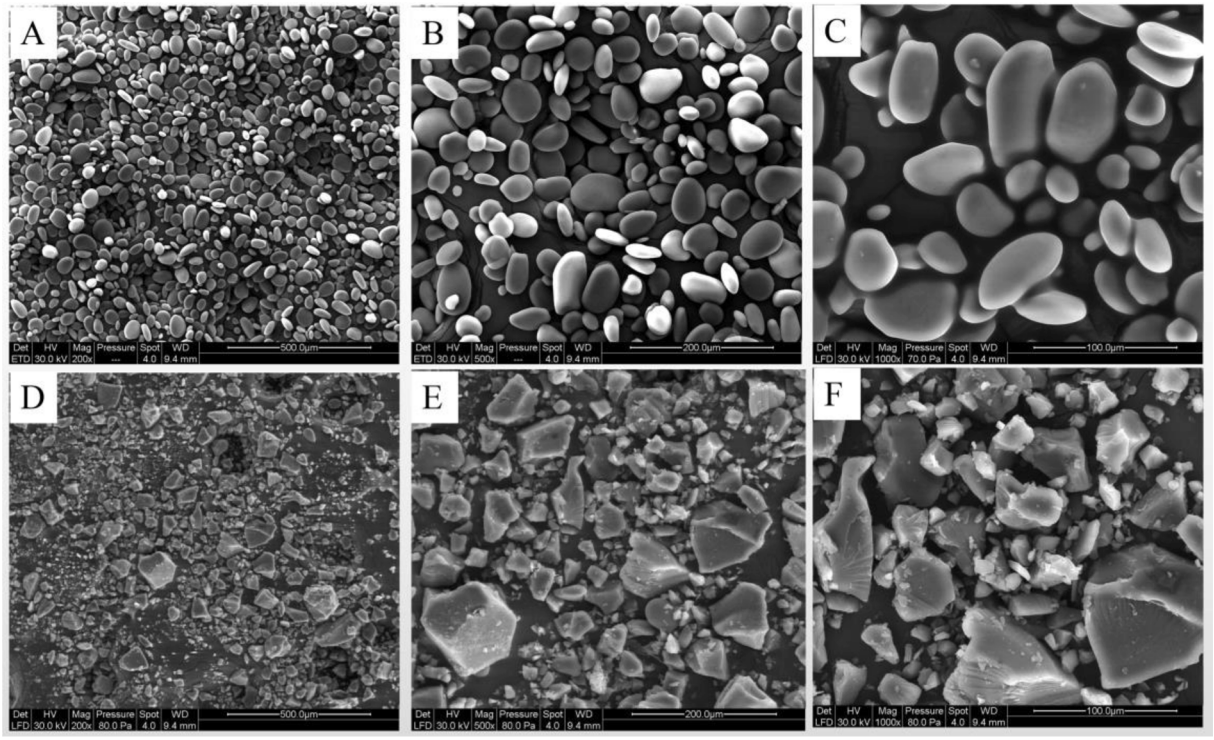

Fig. 1. Scanning electron microscopy (SEM)of NS **(A, B and C)** and Ce-RS3 **(D, E and F).**

diffraction peaks at 17, 15, 22, and 24°, as well as a typical diffraction peak at 5°(2θ), indicating a B-type allomorph (Fig. 2B). After processing, Ce-RS3 maintained the B-type pattern with a similar (2θ) peak position, but displayed more intense and defined peaks. The relative crystallinity changes indicate the extent of interaction between the double helices of starch crystals and the differences in the proportions of microcrystalline filaments (Song & Jane, 2000). To investigate starch crystalline information changes in more detail, the relative crystallinity was determined for NS and Ce-RS3 starches. The relative crystallinity of Ce-RS3 (39.40%) was higher than that of native starch (34.71%), which was consistent with a previous study (Kiatponglarp et al., 2015), which reported that a low recrystallization temperature was beneficial for the formation of B-type polymorphs, and the annealing process could increase crystallinity. Moreover, the relative crystallinity of Ce-RS3 was higher than previously reported (Huang et al., 2016; Mao et al., 2018). The observed higher crystallinity indicated that the Ce-RS3 contained a more ordered double helix structure after double enzymolysis (Song & Jane, 2000). These might be attributed to the release of more low molecular weight linear chain fragments, which was conducive to the formation of a more organized double-helix structure during the regeneration process, thus ultimately improving crystal integrity (Villas-Boas & Franco, 2016; Li, Yuan, & Ai, 2020). Combined with FT-IR analysis, these findings demonstrated that dual enzyme hydrolysis can promote the release and rearrangement of debranched starch chains in native starch, forming more organized double helix structures and improving crystal perfection.

3.1.6. Chain-length distributions (CLDs)

Fig. 2C shows the CLDs of NS and Ce-RS3 after normalization to the global maximum. To better quantify and interpret the CLDs, the chain regions were divided into three parts according to the reported method (Li, Yuan, & Ai, 2020) with some modifications. These three parts include short chains (A chain, DP 6–36), intermediate chains (B chain, DP 37–100) from amylopectin, and long chains (C chain, DP > 100) from amylose or long amylopectin branch chains. After double enzymatic hydrolysis, the peak of long chains (DP > 100) of Ce-RS3 was different from that of native starch, shifting towards low molecular weight chains (Fig. 2C). The summary information of chain length distribution (DP ≤ 100) of debranched starch is shown in Table S3. Compared with native starch, Ce-RS3 exhibited a significant increase in the proportion of medium chains and a decreased in the proportion of short chains (Table S3). Interestingly, no noticeable difference was observed in the average DP of A (DP 6–36) and B (DP 37–100) chains from NS and Ce-RS3, but Ce-RS3 had a significantly higher overall average chain length (DP 6-100) than those of NS. The α-amylase preferentially hydrolyses starch long chains rather than amylopectin within dense clusters (Villas-Boas & Franco, 2016). These results indicated decreased mainly long chains of NS with the attack of amylase before debranching. The long chains were converted into medium chains, and the medium and short chains were partially hydrolyzed. CLDs is a crucial factor for the physicochemical properties of starch granules. Short chains, especially DP 6–23, are not conducive to the formation of thermally stable crystallites during the recrystallization of starch chains (Gidley & Bulpin, 1989), and the presence of long and extremely long chains can reduce the density and stability of crystals and hinder crystallization (Genkina, Wikman, Bertoft, & Yuryev, 2007). Intermediate length chains have higher mobility and a tendency to aggregate and retrogradation (Gidley & Bulpin, 1989; Li, Yuan, & Ai, 2020), the increase of DP 37–100 is associated with an increase in RS3 content, as suggested by (Joo & Wha, 2015), RS3 isolated from heat-moisture treated waxy potato starch had a higher proportion of DP ≥ 37 than those of native and slowly digestible starch + RS. Also, an increase in the proportion of DP 37–100 is more prone to form B-type RS and favors its resistance to digestive enzymes (Jane, Chen, Lee, Mcpherson, & Kasemsuwan, 1999; Joo & Wha, 2015). These data correspond well to the observed differences in the physico-chemical properties of Ce-RS3 and NS.

These results indicated that double enzymatic hydrolysis leads to the release of linear chains of more appropriate sizes, and these chains can easily re-associate and crystallize for altered physical and chemical properties of Ce-RS3. Previous *in vitro* studies have found that double helix structures and crystallinity degrees could affect intestinal flora by

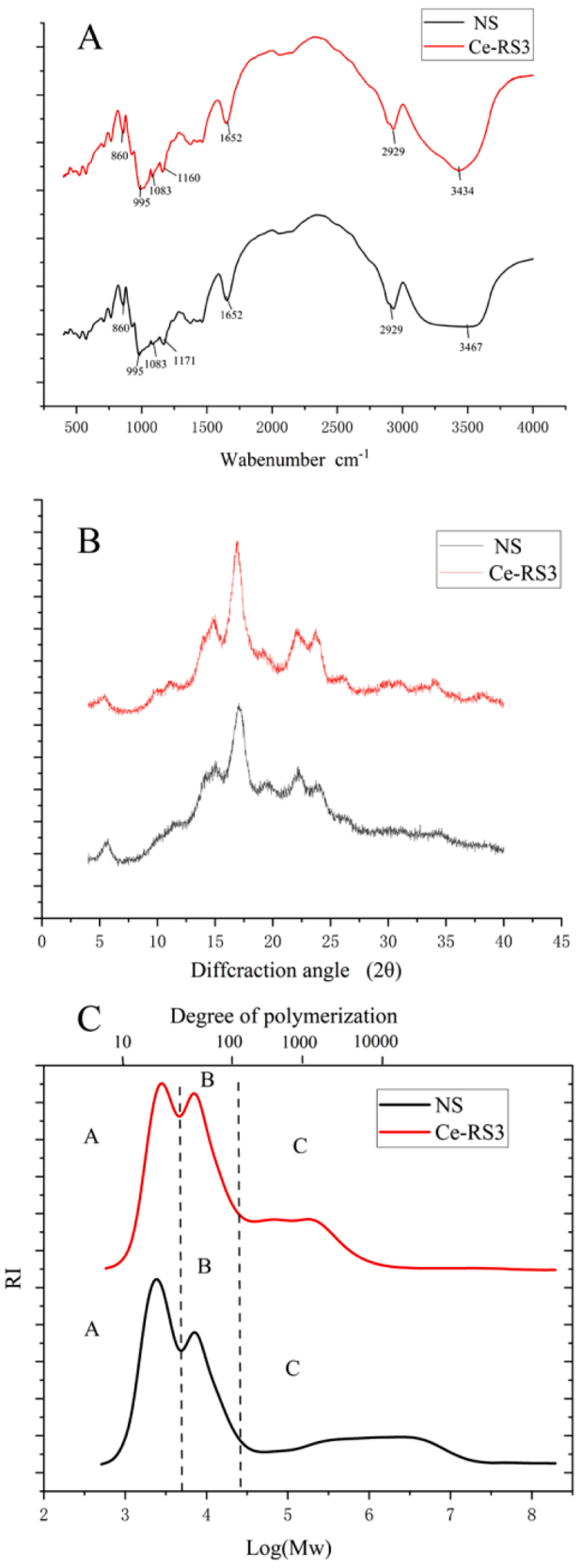

Fig. 2. (A), FT-IR spectra of NS and Ce-RS3; **(B),** X-ray diffraction patterns of NS and Ce-RS3; **(C),** CLDs of NS and Ce-RS3 (All CLDs were normalized to the same global maximum).

altering the accessibility of crystallites to fermentation (Gu, Li, Hamaker, Gilbert, & Zhang, 2020; Lesmes, Beards, Gibson, Tuohy, & Shimoni, 2008), with increased prebiotic properties of RS, especially RS3, with the increased proportion of type B microcrystalline filaments (Dongowski, Jacobasch, & Schmiedl, 2005). Thus, Ce-RS3 might have a physiological function and good gut microbial fermentation properties *in vivo*.

3.2. Anti-hyperlipidemic effect of Ce-RS3

3.2.1. Serum levels of lipids in mice

In this study, dyslipidemia was observed in the mice of the Model group (Fig. 3A), represented by their significantly higher levels of TC, TG, and LDL-C, but significantly lower level of HDL-C, compared with those in normal mice. According to previous studies based on HFD-induced hyperlipidemic mice model, the RS from yam and winged yam exhibited anti-hyperlipidemic activities (Huang et al., 2016; Mao et al., 2018). Here in the present study, high-dose Ce-RS3 significantly reduced the serum levels of TC, TG, and LDL-C, whereas it substantially increased HDL-C after 12 weeks of intervention, demonstrating its anti-hyperlipidemic pharmacological effects. A similar trend was also observed in the low-dose Ce-RS3 group, but the effect was not statistically significant. These results indicated that Ce-RS3 is a promising bioactive starch, which can be potentially used for nutritional intervention strategies to alleviate hyperlipidemia.

3.2.2. Histopathological examination

To investigate the histopathological changes, H&E staining of liver and fat tissues was conducted (Fig. 3C). No histological changes of liver were observed in the untreated mice of the control group. In contrast, the mice in the model group exhibited substantial morphological changes around the liver tissue, which included diffuse vesicular steatosis, aberrant cell arrangement, and enlarged adipocytes, indicating that lipid droplets were largely accumulated in liver. Following simvastatin intervention, the hepatic fatty lesions in the hyperlipidemic mice were dramatically improved and the liver cells were regularly rearranged. Similarly, hepatic injury and fat accumulation in the mice of the model group were substantially ameliorated with high-dose Ce-RS3 intervention. In particular, the morphology of hepatocytes was greatly improved by high-dose Ce-RS3.

Additionally, adipocytes in the mice of the model group were evidently larger with irregular morphology, while their number was notably less, in comparison with those of the normal group. However, the hyperlipidemia-induced adipocyte injury was greatly relieved by simvastatin and Ce-RS3. Further, the effect of Ce-RS3 on adipocytes was assessed using the Image pro-plus 6.0 (IPP) software (Fig. 3B). We observed that the area of adipocytes was markedly reduced by simvastatin and Ce-RS3, with higher effects achieved by treating with simvastatin and high-dose Ce-RS3. Overall, the pathological findings were consistent with those from the above-mentioned biochemical analyses, which validated the anti-hyperlipidemic effect of Ce-RS3.

3.3. Modulation of gut microbiota

Emerging evidence has revealed that metabolic disorders, including hyperlipidemia, have a close relation with gut microbiota changes during the development or progression of the diseases (Vojinovic et al., 2019). Considering the above mentioned findings, the modulatory effect of high-dose Ce-RS3 on gut microbiota of the hyperlipidemic mice was further assessed. Combined with pharmacodynamic and pathological results, only the H_Ce-RS3 group was applied in subsequent analyses.

3.3.1. Gut microbiota composition

A total of 1,376,350 high-quality sequences were obtained from 24 fecal samples, which provided an average of 57,348 ± 6,587 sequences per sample. These sequencing reads were assigned to OTUs with 97%

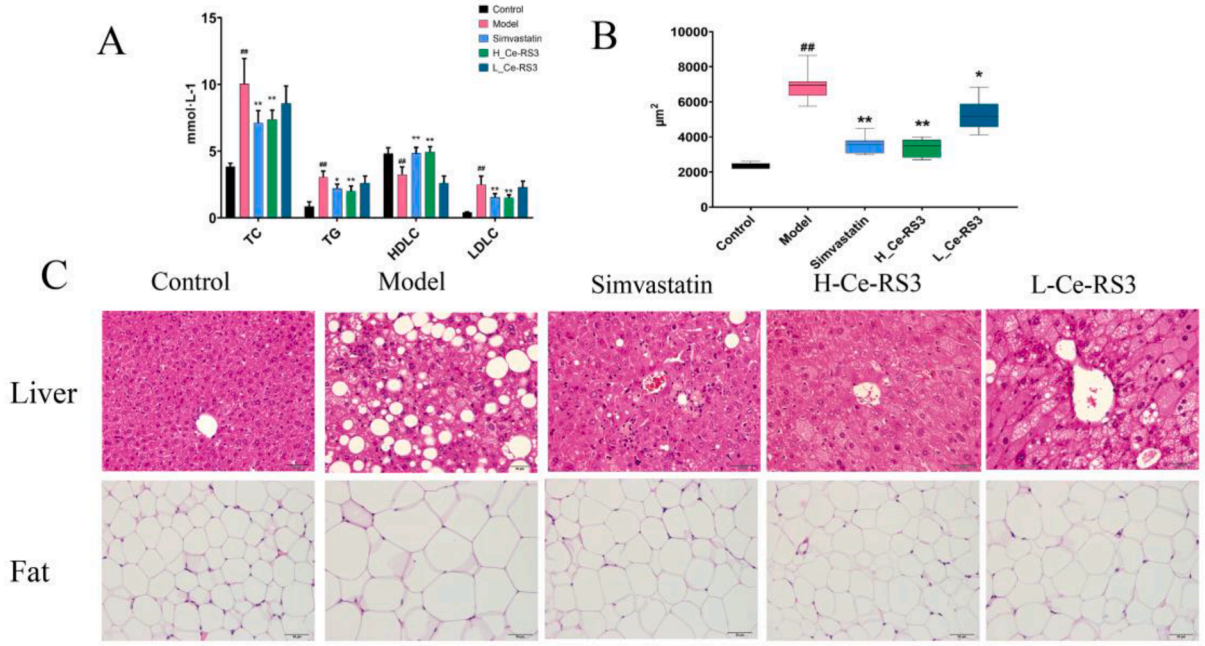

Fig. 3. Anti-hyperlipidemic effects of Ce-RS3; **(A)** Serum lipid levels of TC, TG, LDL-C, HDL-C; **(B)** Effect of Ce-RS3 on the area of adipocytes (HE × 400); **(C)** Histopathological examination of the liver and fat tissue in mice(liver, ×400; Fat × 400) * $p < 0.05$, **$p < 0.01$ Model versus the Control group, # $p < 0.05$, ## $p < 0.01$ Ce-RS3 and simvastatin versus the Model group($x \pm SD$, $n = 6$).

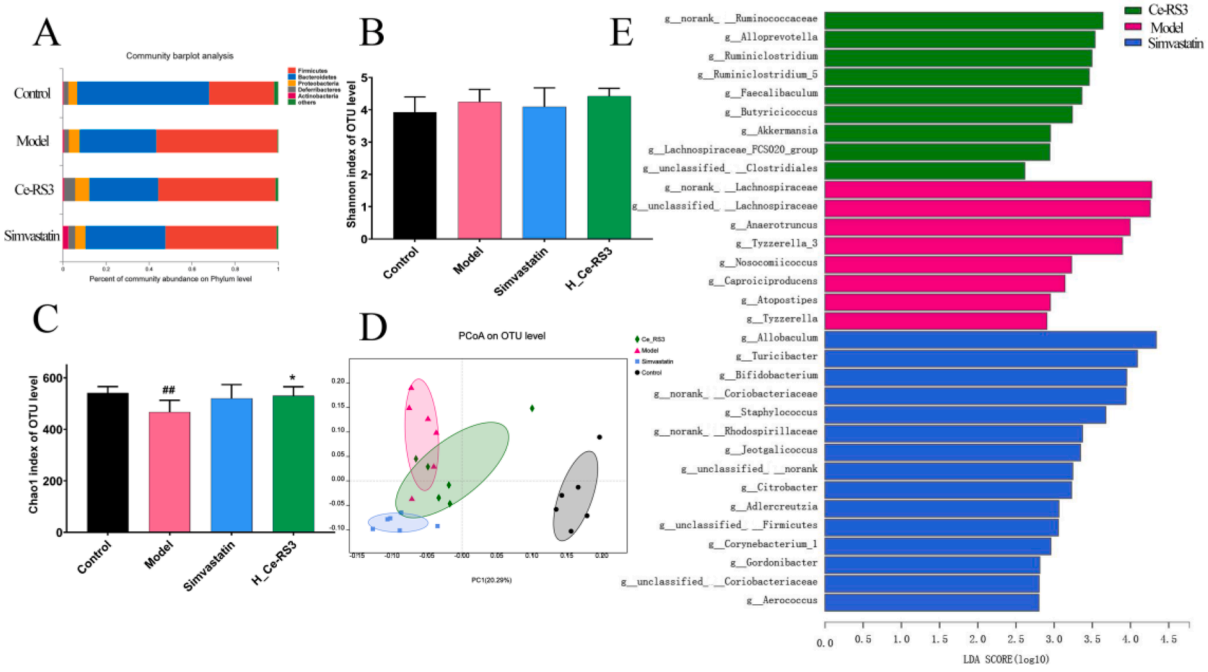

Fig. 4. Gut microbiota structure changes. **(A)** The gut microbiota composition at the phylum; **(B)** Shannon index; **(C)** Chao1 index; **(D)** Unweighted UniFrac distance-based principal coordinate analysis (PCoA; $n = 6$ per group); **(E)** Cladogram of the LEfSe results; Taxonomic represent statistically and biologically consistent differences. Only the taxa with a significant logarithmic LDA threshold score of > 2.5 and $p < 0.05$ were shown.

sequence similarity. The gut bacteria were broadly classified into five phyla, including *Bacteroidetes*, *Firmicutes*, *Proteobacteria*, *Deferribacteres*, and *Actinobacteria*, in which *Bacteroidetes* and *Firmicutes* were dominant (Fig. 4A). Previous research has indicated that metabolic disorder is associated with decreased abundance of *Bacteroidetes* and increased abundance of *Firmicutes* in gut microbiota (Plovier et al., 2016; Zhang et al., 2020). Accordantly, compared with the mice of the normal group, those in the model group had significantly reduced *Bacteroidetes* and increased *Firmicutes*. However, the abundances of these phyla were partially restored by Ce-RS3 and simvastatin intervention.

An overall higher diversity of gut microbiota implies a better gut health, while the reduction of diversity is a common feature shared by the individuals with various metabolic diseases (Plovier et al., 2016; Vojinovic et al., 2019; Zhang et al., 2020). More importantly, gut microbiota can facilitate lipid circulation, and a higher diversity of gut microbiota is significantly associated with a lower TC concentration

(Vojinovic et al., 2019). The diversity microbial structure of gut microbiota was analyzed by examining alpha-diversity indices Shannon and Chao1. The alpha-diversity estimates between the control and model groups were significantly different. HFD-feeding resulted in a significantly lower Chao1 index with no effect on the Shannon index (Fig. 4B and C). Ce-RS3 intervention significantly increased the Chao1 index of the model group. The PCoA plot showed that control and model groups were substantially separated along the PC1 axis, which suggested remarkably different structures of gut microbial community (Fig. 4D). However, treatment with Ce-RS3 and simvastatin reversed the HFD-induced variation, showing microbial changes relative to the model group. Interestingly, although some Ce-RS3 group samples slightly overlapped with those of the Model group, there was a tendency to converge toward the control group on the X-axis, indicating microbial composition might more closely resemble that of the Control group. Overall, distinct bacterial phylogenetic compositions and lower phylotype richness were observed in hyperlipidemic mice compared with control mice. Ce-RS3 modulated gut microbiota dysbiosis and increased ecosystem diversity, which could alleviate hyperlipidemia.

3.3.2. Key bacteria responded to Ce-RS3

To further identify the specific bacterial taxa whose relative abundances were altered significantly, LEfSe method was employed. At the genus level, a total of 32 consistent phylogenetic units were statistically discriminative among groups (Fig. 4E). A total of 8 genera, including *Anaerotruncus*, *Tyzzerella*, *Tyzzerella_3*, *Nosocomiicoccus*, *Caproiciproducens*, *Atopostipes*, *norank Lachnospiraceae*, and *unclassified Lachnospiraceae*, were enriched in the model group. Ce-RS3 had a powerful effect on the abundances of *Alloprevotella*, *Ruminiclostridium*, *Ruminiclostridium_5*, *Faecalibaculum*, *Butyricicoccus*, *Akkermans*, *Lachnospiraceae_FCS020_group*, *unclassified Clostridiales*, and *norank Ruminococcaceae*. Moreover, 15 genera, such as *Allobaculum*, *Bifidobacterium*, and *Staphylococcus*, were enriched in the simvastatin group.

The benefits of RS in modulating host health through fermentation by the colonic microbiota, particularly the production of short-chain fatty acids (SCFAs) by enriched SCFAs-producing bacteria, have been widely recognized (Bindels, Walter, & Ramer-Tait, 2015). SCFAs-producing bacteria can maintain intestinal integrity, provide nutrients to intestinal cells, and reduce gut inflammation (Zhao et al., 2018). Targeted restoration of these SCFAs-producing bacteria is a potential strategy for the prevention and treatment of metabolic disorders (Zhao et al., 2018). In this study, Ce-RS3 markedly enriched several kinds of SCFAs-producing bacteria, including *Alloprevotella*, *Butyricicoccus*, and *Ruminiclostridium* (Antharam et al., 2013; Downes, Dewhirst, Tanner, & Wade, 2013) . However, the SCFAs-producing bacteria identified as enriched by Ce-RS3 were not the same as those previously reported in other RS3 studies. For example, Gu, Li, Hamaker, Gilbert, and Zhang (2020) reported that rice RS3 enriched SCFAs-producing bacteria in the lachnospiraceae family's flora, particularly *Blautia* and *Roseburia*. However, Zeng et al. (2017) found that the administration of RS3 to mice increased *Ruminococcaceae* and *Clostridium*. Overall, the results of studies of RS effects on SCFAs-producing bacteria have not been consistent (Bindels, Walter, & Ramer-Tait, 2015). A potential explanation for these disparate outcomes may be altered fermentation due to different utilization by gut microbiota of RS3 with different fine structures. Gu, Li, Hamaker, Gilbert, and Zhang (2020) have observed that fecal microbiota responses to rice RS3 are specific to the amylose molecular structure. Besides, there is functional redundancy in the production of SCFAs by fecal microbiota (Zhao et al., 2018). Many gut bacterial genera share the genes for producing SCFAs, and the detected changes in specific SCFAs-producing bacteria can vary due to different sampling locations and donors. In this study, very active SCFAs-producing bacteria were observed in the Ce-RS3 group, indicating that Ce-RS3 promotes host health by enriching bacteria that produce SCFAs.

The gut microbiota of the hyperlipidemic mice exhibited an enriched pro-inflammatory bacterial components, including *Tyzzerella*, *Tyzzerella_3*, and *Anaerotruncus* (Fig. 4E); *Tyzzerella* and *Tyzzerella_3* are potential pathogens associated with metabolic disorders, which were previously found to be enriched in mice with obesity (Miao et al., 2018). Increased abundance of *Anaerotruncus* has been associated with elevated pro-inflammatory chemokines and inflammation, suggesting a significant risk factor for metabolic disorders (Conley, Wong, Duyck, Hord, & Sharpton, 2016). However, these trends were improved by Ce-RS3. More importantly, Ce-RS3 intervention increased the abundances of *Akkermansia* and *Faecalibaculum*. *Akkermansia* is a well-known beneficial bacterium with crucial immune metabolism functional roles in the gut intestine, which can combat obesity-related metabolic syndrome (Plovier et al., 2016). *Faecalibaculum* has been reported to possess anti-inflammatory effects and contribute to alleviating inflammatory symptoms in patients with Crohn's disease (Sokol et al., 2008). These characteristic bacteria might be the critical components of the microbiome landscape and help reject conditional pathogens.

3.3.3. Structure-function relationship

Here, we reported that Ce-RS3, a novel type 3 Resistant Starch from *Canna edulis,* significantly alleviated dyslipidemia in hyperlipidemic mice. Many physiological effects have been ascribed to the indigestible characteristics of RS (Bindels, Walter, & Ramer-Tait, 2015), and the anti-hyperlipidemic effect produced by Ce-RS3 may be related to its prebiotic properties as mediated by its inherent and distinct physicochemical properties. Ce-RS3 treatment effectively modulated gut microbiome dysbioses, resulting in increased ecosystem diversity and enhancement of a more balanced community of health-promoting SCFAs producers, contributing to hyperlipidemia improvement (Zhao et al., 2018). These results might be attributed to the fine molecular structures of Ce-RS3. RS3 is better for bacterial fermentation than RS2 (Xu, Ma, Li, Liu, & Hu, 2020). RS3 with type-B crystallites have longer chain double helices and more ordered packing of double helices than those with A and C patterns, making them generally more resistant to amylolytic digestion (Jane, Wong, & Mcpherson, 1997; Ma & Boye, 2018). SEM images revealed that Ce-RS3 has a dense block structure, which may increased its resistance to enzyme attack (Zeng et al., 2018). Thus, Ce-RS3 might improve fermentation in the colon of hyperlipidemic mice, enabling more even distribution of substances in the intestine for full bacterial utilization, resulting in profound effects on the structure of intestinal flora and ultimately regulating host metabolism and lipid homeostasis. This speculation was supported by Xu, Ma, Li, Liu, and Hu (2020) and Lesmes, Beards, Gibson, Tuohy, and Shimoni (2008) that RS3 with B crystallites exhibited better fermentation, with enrichment of SCFAs-producing bacteria and improvement of gut microecological health compared to the fermentation that occurs with other types of RS.

Interestingly, Ce-RS3 enriched different SCFAs-producing bacteria than those reported in other studies (Gu, Li, Hamaker, Gilbert, & Zhang, 2020; Zeng et al., 2017). Besides, Ce-RS3 exhibited a more comprehensive range of gut microbiota regulation by reducing inflammatory bacteria and increasing host-beneficial bacteria, especially *Akkermansia*, changes that have rarely been reported in previous studies (Bindels, Walter, & Ramer-Tait, 2015; Gu, Li, Hamaker, Gilbert, & Zhang, 2020; Xu, Ma, Li, Liu, & Hu, 2020; Zeng et al., 2017). Although the precise mechanism by which Ce-RS3 specifically enhances microbes remains unclear, specific fine structure likely contributes. Ce-RS3 had a higher crystallinity degree and proportion of chains with DP 37–100 compared with other RS3 reported by literature (Gu, Li, Hamaker, Gilbert, & Zhang, 2020; Xu, Ma, Li, Liu, & Hu, 2020), which might be a potential factor for Ce-RS3 to regulate gut microbiota more widely. The prebiotic properties of RS3 increase with B-type microcrystalline filaments (Gerhard, Gisela, & Detlef, 2005). Besides, differences in the proportion of chains, especially DP 37–100, have been found to exert a substantial impact on the microbial community at the genus level (Gu, Li, Hamaker, Gilbert, & Zhang, 2020). The higher proportion of chains with DP 37–100 is conducive to a broader enrichment of specific beneficial bacteria. These findings expanded Ce-RS3′s potential beneficial

microbial mechanisms by regulating immune and inflammatory mediators in addition to SCFAs and suggested a potential specific regulatory effect of Ce-RS3 fine molecular structure on the microbiota. Overall, Ce-RS3 prepared by double enzymatic hydrolysis significantly improved host microbiota composition, producing prebiotic properties by selective utilization by host microorganisms.

4. Conclusions

The present study demonstrates that dual enzymatic hydrolysis, combined with recrystallization, is a simple, green, and efficient method to process Ce-RS3 for large-scale industrial production. The content of Ce-RS3 under optimal processing conditions is 49.11%. Processing disrupted the Ce-RS3 granules, with increased degree of crystallinity and orderliness, and a higher proportion of DP 37–100. The structural modification increased the prebiotic properties of Ce-RS3. Ce-RS3 exhibits significant anti-hyperlipidemic activity with decreasing TG, TC, and LDL-C and increasing HDL-C, to alleviate liver fatty lesions, inhibit adipocyte enlargement, and suppress fat accumulation. These beneficial effects are closely related to specific changes of intestinal microorganisms, including increased gut microbial diversity and unique microbial enrichment, potentially mediated by the fine structure of Ce-RS3. These observations should enable industrial production of Ce-RS3 for use as prebiotic, and future work should investigate the fine structure-gut microbiota- physiological functions of RS.

Funding

This work was supported by the Beijing Municipal Natural Science Foundation (No.7192120); the National Science & Technology Fundamental Resources Investigation Program of China (No.2018FY100700); and the Science & Technology Support Plan of Guizhou Province (No.20172546, No.20204Y074).

CRediT authorship contribution statement

Chi Zhang: Conceptualization, Data curation, Methodology, Writing - original draft. **Minyi Qiu:** Conceptualization, Data curation, Methodology. **Ting Wang:** Formal analysis, Software. **Linglong Luo:** Formal analysis, Software. **Wenjuan Xu:** Formal analysis, Software. **Jiahui Wu:** Formal analysis, Software. **Fangyuan Zhao:** Formal analysis, Software. **Kaiyang Liu:** Formal analysis, Software. **Yuan Zhang:** Writing - review & editing, Funding acquisition. **Xueyong Wang:** Writing - review & editing, Funding acquisition.

Declaration of Competing Interest

The authors declare that they have no known competing financial interests or personal relationships that could have appeared to influence the work reported in this paper.

Acknowledgment

We are grateful to Guizhou YiLiTai Biotechnology Co., Ltd. and Guizhou BencaoHeshan Functional Food Co., Ltd. for kindly supplying starch raw materials. Besides, we wish to thank Dr. Shisheng Wang (West China Hospital, Sichuan University) and Dr. Chengpin Shen (Omicsolution Co., Ltd) for their data analysis suggestions.

Appendix A. Supplementary data

Supplementary data to this article can be found online at https://doi.org/10.1016/j.foodchem.2021.129340.

References

Antharam, V. C., Li, E. C., Ishmael, A., Sharma, A., Mai, V., Rand, K. H., et al. (2013). Intestinal dysbiosis and depletion of butyrogenic bacteria in Clostridium difficile infection and nosocomial diarrhea. *Journal of Clinical Microbiology, 51*(9), 2884–2892.

Bindels, L. B., Walter, J., & Ramer-Tait, A. E. (2015). Resistant starches for the management of metabolic diseases. *Current Opinion in Clinical Nutrition & Metabolic Care, 18*(6), 559–565.

Cai, L., & Shi, Y.-C. (2013). Self-assembly of short linear chains to A- and B-type starch spherulites and their enzymatic digestibility. *Journal of Agricultural & Food Chemistry, 61*(45), 10787–10797.

Conley, M. N., Wong, C. P., Duyck, K. M., Hord, N., & Sharpton, T. J. (2016). Aging and serum MCP-1 are associated with gut microbiome composition in a murine model. Peer J, 4, e1854.

Dongowski, G., Jacobasch, G., & Schmiedl, D. (2005). Structural stability and prebiotic properties of resistant starch type 3 increase bile acid turnover and lower secondary bile acid formation. *Journal of Agricultural & Food Chemistry, 53*(23), 9257–9267.

Downes, J., Dewhirst, F. E., Tanner, A., & Wade, W. G. (2013). Description of Alloprevotella rava gen. nov., sp. nov., isolated from the human oral cavity, and reclassification of Prevotella tannerae Moore et al. 1994 as Alloprevotella tannerae gen. nov., comb. nov. International Journal of Systematic and Evolutionary Microbiology, 63, 1214-1218.

Genkina, Natalia K., Wikman, Jeanette, Bertoft, Eric, & Yuryev, Vladimir P. (2007). Effects of structural imperfection on gelatinization characteristics of amylopectin starches with A-and B-type crystallinity. *Biomacromolecules, 8*(7), 2329–2335.

Gerhard, D., Gisela, J., & Detlef, S. (2005). Structural stability and prebiotic properties of resistant starch type 3 increase bile acid turnover and lower secondary bile acid formation. *Journal of Agricultural and Food Chemistry, 53*, 9257–9267.

Gidley, Michael J., & Bulpin, Paul V. (1989). Aggregation of amylose in aqueous systems: The effect of chain length on phase behavior and aggregation kinetics. *Macromolecules, 22*(1), 341–346.

Gu, Fangting, Li, Cheng, Hamaker, Bruce R., Gilbert, Robert G., & Zhang, Xiaowei (2020). Fecal microbiota responses to rice RS3 are specific to amylose molecular structure. *Carbohydrate Polymers, 243*, 116475. https://doi.org/10.1016/j.carbpol.2020.116475.

Huang, H., Jiang, Q., Chen, Y., Li, X., Mao, X., Chen, X., et al. (2016). Preparation, physico-chemical characterization and biological activities of two modified starches from yam (Dioscorea Opposita Thunb.). *Elsevier, 55*, 244–253.

Hung, Pham Van, & Morita, Naofumi (2005). Physicochemical properties and enzymatic digestibility of starch from edible canna (Canna edulis) grown in Vietnam. *Carbohydrate polymers, 61*(3), 314–321.

Jane, J., Chen, Y. Y., Lee, L. F., McPherson, A. E., Wong, K. S., Radosavljevic, M., et al. (1999). Effects of amylopectin branch chain length and amylose content on the gelatinization and pasting properties of starch. *Cereal Chemistry, 76*(5), 629–637.

Jane, Jay-lin, Wong, Kit-sum, & McPherson, Andrew E. (1997). Branch-structure difference in starches of A- and B-type X-ray patterns revealed by their Naegeli dextrins. *Carbohydrate Research, 300*(3), 219–227.

Jiang, F., Du, C., Jiang, W., Wang, L., & Du, S. K. (2019). The preparation, formation, fermentability, and applications of resistant starch. *International Journal of Biological Macromolecules, 150*, 1155–1161.

Joo, L. C., & Moon, M. T. Wha (2015). Structural characteristics of slowly digestible starch and resistant starch isolated from heat-moisture treated waxy potato starch. *Carbohydrate Polymers, 125*, 200–205.

Lesmes, Uri, Beards, Emma J., Gibson, Glenn R., Tuohy, Kieran M., & Shimoni, Eyal (2008). Effects of resistant starch type III polymorphs on human colon microbiota and short chain fatty acids in human gut models. *Journal of Agricultural and Food Chemistry, 56*(13), 5415–5421.

Li, Liying, Yuan, Tommy Z., & Ai, Yongfeng (2020). Development, structure and in vitro digestibility of type 3 resistant starch from acid-thinned and debranched pea and normal maize starches. *Food Chemistry, 318*, 126485. https://doi.org/10.1016/j.foodchem.2020.126485.

Ma, Zhen, & Boye, Joyce I. (2018). Research advances on structural characterization of resistant starch and its structure-physiological function relationship: A review. *Critical Reviews in Food Science and Nutrition, 58*(7), 1059–1083.

Mao, Xinhui, Lu, Jun, Huang, Hanhan, Gao, Xiaoxiao, Zheng, Hong, Chen, Yuling, et al. (2018). Four types of winged yam (Dioscorea alata L.) resistant starches and their effects on ethanol-induced gastric injury in vivo. *Food Hydrocolloids, 85*, 21–29.

Miao, L., Yang, S., Peng, L., Xin, S., Pan, J., He, J., et al. (2018). Combined Use of C. butyricum Sx-01 and L. salivarius C-1-3 Improves Intestinal Health and Reduces the Amount of Lipids in Serum via Modulation of Gut Microbiota in Mice. *Nutrients, 10*, 810.

Plovier, H., Everard, A., Druart, C., Depommier, C., Van Hul, M., Geurts, L., et al. (2016). A purified membrane protein from Akkermansia muciniphila or the pasteurized bacterium improves metabolism in obese and diabetic mice. *Nature Medicine, 23*, 107.

Shi, Miaomiao, Chen, Yun, Yu, Shujuan, & Gao, Qunyu (2013). Preparation and properties of RS III from waxy maize starch with pullulanase. *Food Hydrocolloids, 33*(1), 19–25.

Singh, Narpinder, Inouchi, Naoyoshi, & Nishinari, Katsuyoshi (2006). Structural, thermal and viscoelastic characteristics of starches separated from normal, sugary and waxy maize. *Food Hydrocolloids, 20*(6), 923–935.

Sokol, H., Pigneur, B., Watterlot, L., Lakhdari, O., Bermudez-Humaran, L. G., Gratadoux, J.-J., et al. (2008). Faecalibacterium prausnitzii is an anti-inflammatory commensal bacterium identified by gut microbiota analysis of Crohn disease

patients. *Proceedings of the National Academy of Sciences of the United States of America, 105*(43), 16731–16736.
Song, Y., & Jane, J. (2000). Characterization of barley starches of waxy, normal, and high amylose varieties. *Carbohydrate Polymers, 41*(4), 365–377.
Villas-Boas, Flávia, & Franco, Célia M. L. (2016). Effect of bacterial β-amylase and fungal α-amylase on the digestibility and structural characteristics of potato and arrowroot starches. *Food Hydrocolloids, 52*, 795–803.
Vojinovic, Dina, Radjabzadeh, Djawad, Kurilshikov, Alexander, Amin, Najaf, Wijmenga, Cisca, Franke, Lude, et al. (2019). Relationship between gut microbiota and circulating metabolites in population-based cohorts. *Nature Communications, 10*(1). https://doi.org/10.1038/s41467-019-13721-1.
Kiatponglarp, Worawikunya, Tongta, Sunanta, Rolland-Sabaté, Agnès, & Buléon, Alain (2015). Crystallization and chain reorganization of debranched rice starches in relation to resistant starch formation. *Carbohydrate Polymers, 122*, 108–114.
Xu, Jiangbin, Ma, Zhen, Li, Xiaoping, Liu, Liu, & Hu, Xinzhong (2020). A more pronounced effect of type III resistant starch vs. type II resistant starch on ameliorating hyperlipidemia in high fat diet-fed mice is associated with its supramolecular structural characteristics. *Food & Function, 11*(3), 1982–1995.
Zaman, S. A., & Sarbini, S. R. (2015). The potential of resistant starch as a prebiotic. *Critical Reviews in Biotechnology, 7*, 578–584.
Zeng, Hongliang, Chen, Peilin, Chen, Chuanjie, Huang, Cancan, Lin, Shan, Zheng, Baodong, et al. (2018). Structural properties and prebiotic activities of fractionated lotus seed resistant starches. *Food Chemistry, 251*, 33–40.
Zeng, H., Huang, C., Lin, S., Zheng, M., Chen, C., Zheng, B., et al. (2017). Lotus Seed Resistant Starch Regulates Gut Microbiota and Increases SCFAs Production and Mineral Absorption in Mice. *Journal of Agricultural & Food Chemistry, 42*, 9217–9225.
Zhang, Chi, Ma, Shuangshuang, Wu, Jiahui, Luo, Linglong, Qiao, Sanyang, Li, Ruxin, et al. (2020). A specific gut microbiota and metabolomic profiles shifts related to antidiabetic action: The similar and complementary antidiabetic properties of type 3 resistant starch from Canna edulis and metformin. *Pharmacological Research, 159*, 104985. https://doi.org/10.1016/j.phrs.2020.104985.
Zhang, Huanxin, & Jin, Zhengyu (2011). Preparation of products rich in resistant starch from maize starch by an enzymatic method. *Carbohydrate Polymers, 86*(4), 1610–1614.
Zhang, Juan, Chen, Feng, Liu, Feng, & Wang, Zheng-Wu (2009). Study on structural changes of microwave heat-moisture treated resistant Canna edulis Ker starch during digestion in vitro. *Food Hydrocolloids, 24*(1), 27–34.
Zhang, Juan, & Wang, Zheng-Wu (2009). Optimization of reaction conditions for resistant Canna edulis Ker starch phosphorylation and its structural characterization. *Industrial Crops & Products, 30*(1), 105–113.
Zhang, Yi, Zeng, Hongliang, Wang, Ying, Zeng, Shaoxiao, & Zheng, Baodong (2014). Structural characteristics and crystalline properties of lotus seed resistant starch and its prebiotic effects. *Food Chemistry, 155*, 311–318.
Zhao, Liping, Zhang, Feng, Ding, Xiaoying, Wu, Guojun, Lam, Yan Y., Wang, Xuejiao, et al. (2018). Gut bacteria selectively promoted by dietary fibers alleviate type 2 diabetes. *Science, 359*(6380), 1151–1156.